RSC Advances

ROYAL SOCIETY OF CHEMISTRY

www.rsc.org/advances

Cite this: DOI: 10.1039/c0xx00000x

www.rsc.org/xxxxxx

ARTICLE TYPE

Highly Electrocatalytic Activity of $W_{18}O_{49}$ Nanowire for Cobalt Complex and Ferrocenium Redox Mediators

Huawei Zhou[a], Yantao Shi[a,]*, Qingshun Dong[a], Liang Wang[a], Hong Zhang,[a], Tingli Ma[b,]*

Received (in XXX, XXX) Xth XXXXXXXXX 20XX, Accepted Xth XXXXXXXXX 20XX

DOI: 10.1039/b000000x

Understanding the relationship between the surface of electrocatalysts and the catalytic properties for different redox mediators is beneficial to the rational design of efficient catalysts for use in practical catalytic processes. Although previous research observed that surface oxygen vacancies (SOVs) affected the catalytic activity for triiodide/iodide (I^-/I_3^-) and T_2/T^- (T^-=5-mercapto-1-methyltetrazole ion) redox mediators in dye-sensitized solar cells (DSCs). However, the electrocatalytic properties of larger and steric metal complex redox mediators (cobalt complex, ferrocenium **)** on SOVs of $W_{18}O_{49}$ are unclear and never been reported. In this study, we investigated the electrocatalytic properties of cobalt complex and ferrocenium redox mediators on SOVs of $W_{18}O_{49}$. Results indicated that the catalytic performance of $W_{18}O_{49}$ nanowires (NWs) as a counter electrode for cobalt complex and ferrocenium redox mediators was comparable to that of Pt. After SOVs filling, the reduction reaction activity of cobalt complex decreases slightly whereas it increases slightly for ferrocenium. These findings enrich our understanding of heterogeneous catalytic reactions on the surface of transition metal complex for different redox mediators.

Introduction

As a result of global warming and the exhaustion of petroleum resources, developing renewable energy has become one of the major scientific issues and challenges. Photoelectrochemical cells[1] and water splitting[2] are attractive methods to scientists and manufactures. As the central component of photoelectrochemical cells or water splitting devices, redox mediators take the function of electron transfer and dye regeneration.[3] Iodide/triiodine redox mediator (I^-/I_3^-) is the most commonly used electrolyte in dye-sensitized solar cells (DSCs).[4] In recent years, other redox mediators have been developed for matching with dyes, thereby yielding high power conversion efficiency (PCE). Lately, DSCs incorporating cobalt-complex as redox mediator and porphyrin as sensitizer achieved a record-setting PCE of 13%.[5] In addition, other metal complex redox (Fe, Cu, and Ni) and organic redox mediators have also been designed and used in DSCs.[6]

The counter electrode (CE) of DSCs is used to collect electrons from the external circuit and for electrocatalytic reduction of redox mediators. Although Pt is the most widely used CE catalyst for iodine/iodide redox mediators, several disadvantages limit its practical application. The scarcity and high cost of Pt cannot meet the needs of mass industrial production. On the other hand, Pt is not always the best catalyst for all redox mediators. For example, Pt is an inefficient catalyst for alkali metal polysulfide electrolyte (S^{2-}/S_n^{2-}), which is used in quantum dot solar cells (QDSCs),[7] or for organic disulfide electrolyte, which is used in DSCs.[8] Therefore, the development of low-cost, high-performance catalysts is highly desirable to replace the Pt used in energy conversion.[9-11]

Tungsten oxides, which are important transition metal compounds, have various practical applications in many fields, such as in optical devices, gas sensors, and catalysts.[12] In the field of catalysts, tungsten oxides are also a hot research topic because of their notable catalytic properties.[13-17] Our group reported that WO_2 nanorods showed excellent catalytic activity for the reduction of triiodide to iodide in DSCs, while WO_3 was inefficient catalysts as CE.[18] Lee et al. reported the use of ordered mesoporous tungsten suboxide as a catalyst for a CE in T_2/T^- (T^- =5-mercapto-1-methyltetrazole ion) electrolyte-based DSCs.[19] They confirmed that the partial reduction of tungsten oxide had a powerful effect on the catalytic activity for T_2/T^- mediator. Yang et al transformed electrocatalytically inactive commercial WO_3 into an efficient CE material for I^-/I_3^- mediator via facile hydrogen treatment.[20] Recently, we found that oxygen-vacancy-rich $W_{18}O_{49}$ was an efficient catalyst when used as CEs in DSCs for both I^-/I_3^- and T_2/T^- redox mediators.[8] However, the influence of SOVs on the electrocatalytic properties of larger redox mediators with steric molecular configurations (cobalt complex, ferrocenium **)** redox mediators in DSCs is unclear.

In this study, electrocatalytic properties of $Co(bpy)_3^{2+}/Co(bpy)_3^{3+}$ (bpy=2,2´-bipyridyl) and Fc/Fc^+ (Fc=ferrocene) on SOVs of $W_{18}O_{49}$ were investigated. Results indicated that the catalytic performance of $W_{18}O_{49}$ nanaowires

(NWs) as a counter electrode for cobalt complex and ferrocenium redox mediators was comparable to that of Pt.

Unlike notable dependence on SOVs for small I^-/I_3^-, the electrocatalytic activity for larger redox mediators with steric molecular configurations (cobalt complex and ferrocenium) demonstrated less dependence on SOVs. The reduction reaction activity of cobalt complex decreased slightly after SOVs filling. By contrast, the reduction reaction activity of ferrocenium increased slightly after SOVs filling. These findings clarified the catalytic properties of SOVs for larger and steric metal complex redox mediators and were helpful for the rational search for highly active Pt-like catalysts for use with different redox mediators.

Experimental section:

Synthesis of $W_{18}O_{49}$ nanowires:

$W_{18}O_{49}$ nanowires were synthesized via the solvothermal utilizing WCl_6 (0.1 g) in ethanol (50 ml) at 180 ºC for 24 hours.[21] WCl_6 was dissolved in ethanol to form clear yellow solution that was then transferred into a Teflon-lined autoclave. After being heated at 180 °C for 24 h, the mixture was cooled to room temperature naturally. The product was collected by centrifugation and washed repeatedly with water and ethanol, finally followed by vacuum drying at 45°C overnight.

Preparation of catalysts electrode:

W-O_V-W: As-synthesized $W_{18}O_{49}$ powders were dispersed in isopropanol. Then obtained suspension was sprayed on FTO glass (0.8cm×10cm). The obtained films were sintered in nitrogen atmosphere at 500 °C for 30 min.

W-O-W: In order to prevent disturbance in operation, a half of electrodes in W-O_V-W was cut for oxidation treatment. Then, the cut electrode was transferred to tube furnace, whose ends are open to air. Filling SOVs was carried out at 350℃ for 1h. Then the electrodes were cooled to room temperature. If increasing the treatment temperature, the $W_{18}O_{49}$ were converted to WO_3 with light yellow.

Pt electrode: The noble metal Pt electrodes were fabricated by pyrolysis H_2PtCl_6 on fluorine-doped tin oxide (FTO) glass as previously reported.[22, 23]

Electrolyte composition for CV:

The cobalt redox couple was synthesized by the literature method.[24] The electrolyte based on $[Co(bpy)_3][ClO_4]_2$/$[Co(bpy)_3][(bpy)_3]_3[ClO_4]_3$ redox mediator was composed of 10 mM $LiClO_4$, 10 mM $[Co(bpy)_3][ClO_4]_2$ and 1 mM $NOBF_4$ in acetonitrile. The electrolyte based on Fc / $FcPF_6$ redox mediator was composed of 10mM $LiClO_4$, 10mM Fc and 1 mM ferrocenium hexafluorophosphate ($FcPF_6$) in acetonitrile.

Electrolyte composition for Tafel, EIS and DSCs:

The electrolyte based on $[Co(bpy)_3][ClO_4]_2$/$[Co(bpy)_3][(bpy)_3]_3[ClO_4]_3$redox mediator was composed of 0.2 M $LiClO_4$, 0.1 M $[Co(bpy)_3][ClO_4]_2$, 0.01 M $NOBF_4$ and 0.5 M 4-tert-butyl pyridine in acetonitrile. The electrolyte based on Fc/$FcPF_6$ redox mediator was composed of 0.1 M $LiClO_4$, 0.1 M Fc, 0.05 M $FcPF_6$, 0.5 M and 4-tert-butyl pyridine in acetonitrile.

Solar cell fabrication:

A layer of 20 nm-sized TiO_2 (P25, Degussa, Germany) layer was printed on FTO glass.[25] When the obtained films sintered at 500 °C were cooled to 90 °C, they were immersed in a solution of N719 dye (5 x 10^{-4} M) in acetonitrile/tert-butyl alcohol (1:1 volume ration) for 22 h or YD2-*o*-C8 dye (6 x 10^{-4} M) in ethanol for 5 h. The architecture of DSCs was assembled by sandwiching electrolyte with a sensitized TiO_2 photoanode and a counter electrode. Compact TiO_2 blocking layer is prepared according to literature.[26]

Characterizations:

XRD patterns were obtained using PANalyticalX´Pert diffractometer (Cu Kα radiation at λ = 1.54 Å) sampling at 2°/ min, 40 kV and 100 mA. Nanostructures of our samples were characterized and analysed by scanning electron microscopy (SEM, Nova Nano SEM 450). The films thicknesses were measured using film-thickness measuring device (Surfcom 130A, Japan). X-ray photoelectron spectra (XPS) was carried out in Thermo ESCALAB 250. The photocurrent–voltage performance of the DSCs was measured by a Keithley digital source meter (Keithley 2601, USA) equipped with a solar simulator (PEC-L15, Peccell, Yokohama, Japan). EIS experiments were measured in the dummy cells in the dark using a computer-controlled potentiostat (ZenniumZahner, Germany). Tafel polarization measurements were carried out with an electrochemical workstation system (CHI630, Chenhua, and Shanghai) in a symmetrical dummy cell. Effective area of the symmetrical cells in the EIS and Tafel-polarization tests was 0.64 cm^2.

Results and discussion

The energy levels and structures of $Co(bpy)_3^{2+}/Co(bpy)_3^{3+}$ and Fc/Fc^+ redox mediators are shown in Figures 1a to 1c. $W_{18}O_{49}$ NWs are prepared by means of a solvothermal approach.[8] $W_{18}O_{49}$ NWs CEs are then prepared by spraying its suspension onto FTO glass. The CE with abundant SOVs is designated as W-O_V-W. Another CE treated by means of in situ filling of SOVs (Figure 1e) in W-O_V-W CEs is designated as W-O-W. Details of the preparation of W-O_V-W and W-O-W CEs are included in the experimental section. Compared with W-O_V-W CE (Figure 1d), W-O-W CE (see SEM image in Figure S1) shows no obvious changes in morphology. The X-ray diffraction pattern shown in Figure S2 further confirms that the tungsten oxide can be assigned to monoclinic $W_{18}O_{49}$, which has the largest oxygen vacancies within the range of $WO_{2.625}$ to WO_3.[21] Furthermore, no crystalline phase variation can be found after SOVs filling. The X-ray photoelectron spectroscopy fitting results (Figure S3) clearly shows that most of the SOVs on $W_{18}O_{49}$ NWs have been eliminated for W-O-W CE. SOVs filling and maintenance of the morphology and crystal phase result in an accurate investigation of the electrocatalytic properties of $Co(bpy)_3^{2+}/Co(bpy)_3^{3+}$ and Fc/Fc^+ redox mediators on SOVs.

Cite this: DOI: 10.1039/c0xx00000x

www.rsc.org/xxxxxx

ARTICLE TYPE

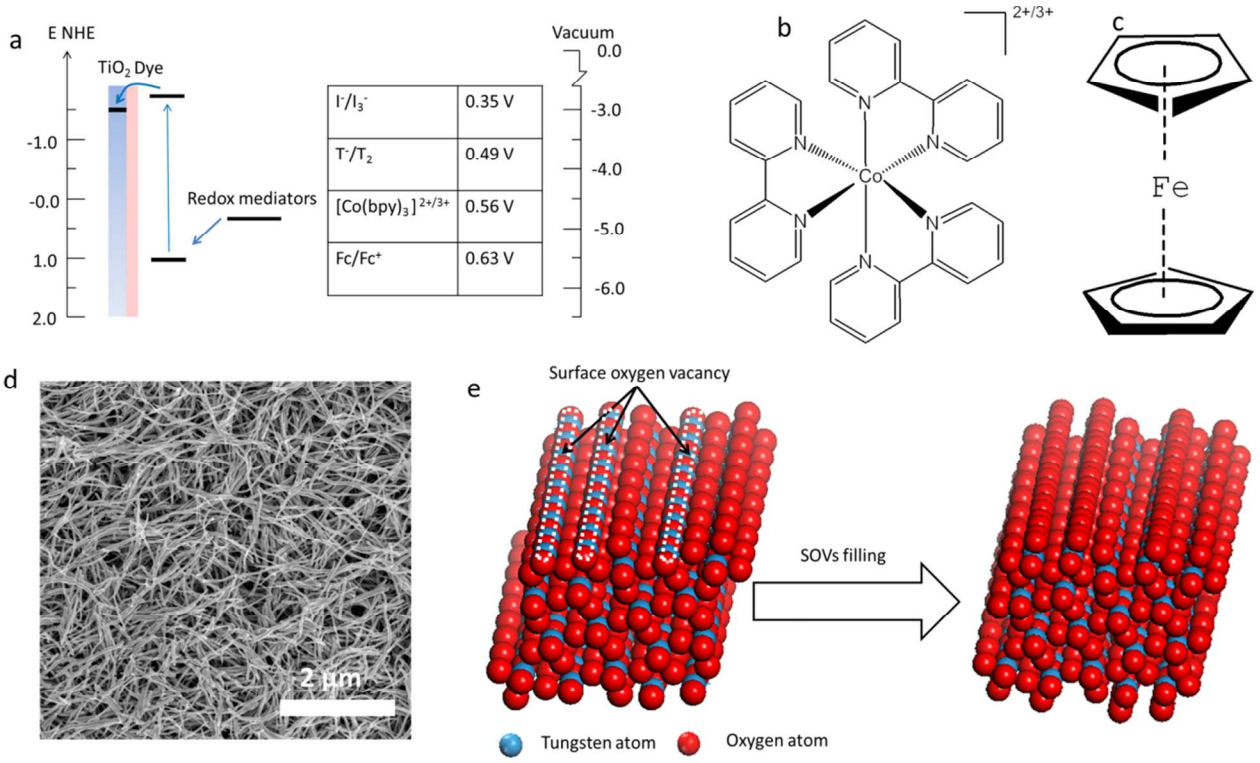

Figure 1. a)Schematic energy digagram for DSCs. The insert table is the energy level for $Co(bpy)_3^{2+}/Co(bpy)_3^{3+}$ and Fc/Fc^+. b) and c) is molecular structures for $Co(bpy)_3^{2+/3+}$ and Fc, respectivly. d) SEM of W-O_V-W. e) Schematic SOVs filling on $W_{18}O_{49}$

Electrocatalytic characterizations are performed to investigate the electrocatalytic properties of $Co(bpy)_3^{2+}/Co(bpy)_3^{3+}$ and Fc/Fc^+ redox mediators on SOVs of $W_{18}O_{49}$. Cyclic voltammetry (CV) is used to examine the electrocatalytic activity of $Co(bpy)_3^{2+}/Co(bpy)_3^{3+}$ and Fc/Fc^+ redox mediators on three different CEs: W-O_V-W, W-O-W, and Pt. Detailed CV characterizations are summarized in Table 1. As shown in Figure 2a, only one pair of redox peaks are observed for $Co(bpy)_3[ClO_4]_2/Co(bpy)_3[ClO_4]_3$ on three catalytic electrodes. The anodic and cathodic peak separation (ΔE_P) of W-O_V-W CE is only 158 mV, approaching that of Pt (153 mV) and indicating high reversibility. In addition, no obvious changes in ΔE_P are observed after SOVs filling. The cathodic peak and anodic peak current current is slightly decreased. For Fc/Fc^+ redox mediators, one pair of redox peaks was also observed on three catalytic electrodes. The ΔE_P of W-O_V-W CE is also close to that of Pt and implying high electrocatalytic activity for Fc/Fc^+. In addition, the electrocatalytic properties of Fc/Fc^+ is different response to SOVs, as shown in Figure 2b and Table 1. The ΔE_P of Fc/Fc^+ decreases slightly rather than increases after SOVs filling, which implies that electrocatalytic activity increases slightly after SOVs filling.

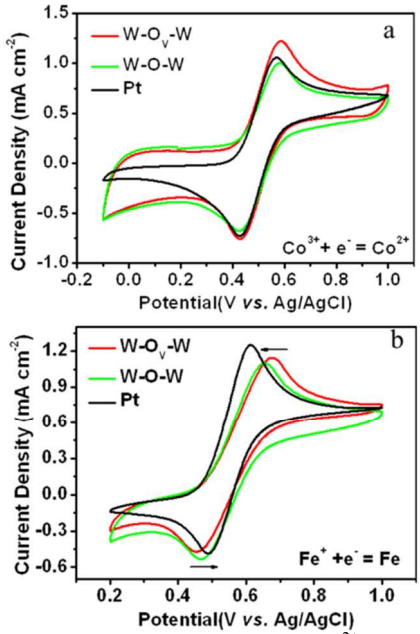

Figure 2. Cyclic voltammograms of $Co(bpy)_3^{2+}/Co(bpy)_3^{3+}$ and Fc/Fc^+ redox mediators on three different electrodes.

To verify the electrocatalytic properties of $Co(bpy)_3^{2+}/Co(bpy)_3^{3+}$ and Fc/Fc^+ redox mediators on SOVs of $W_{18}O_{49}$, Tafel-polarization was conducted with symmetrical cells consisting of two identical CEs. The values of the exchange current density (J_0) in the Tafel zone were obtained, as shown in Table 1. J_0 can be related to charge transfer resistance (R_{ct}) using Equation (1):

$$R_{ct} = \frac{RT}{nFJ_0} \quad (1)$$

where R denotes the gas constant, T stands for the temperature, F represents Faraday's constant, and n denotes the number of electrons involved in the reaction at the electrode. According to Equation (1), the small value of J_0 causes a large R_{ct}. As shown in Figure 3a and table 1, the values of J_0 for W-O_V-W and W-O-W are higher than that of Pt, which indicated that they exhibited high electrocatalytic activity for $Co(bpy)_3^{2+}/Co(bpy)_3^{3+}$. In addition, when the thickness of W-O_V-W for $Co(bpy)_3^{2+}/Co(bpy)_3^{3+}$ increased, the notable decreased in the Tafel zone could be attributed to the large mass transports in the thick film (Figure S4). After SOVs filling, the value of J_0 slightly decreased, which demonstrated that electrocatalytic activity of $Co(bpy)_3^{2+}/Co(bpy)_3^{3+}$ was less dependent on SOVs of $W_{18}O_{49}$. For Fc/Fc^+ redox mediator, the value of J_0 for W-O_V-W and W-O-W were approaching to that of Pt. By contrast, the value of J_0 increased from 0.39 to 0.55 mA cm^{-2} after SOVs filling, which indicated that reduction of SOVs on $W_{18}O_{49}$ was benefited to enhance electrocatalytic activity for Fc/Fc^+. The above results verified the different effects of SOVs on the electrocatalytic properties of $Co(bpy)_3^{2+}/Co(bpy)_3^{3+}$ and Fc/Fc^+ redox mediators and agreed with the results of CV.

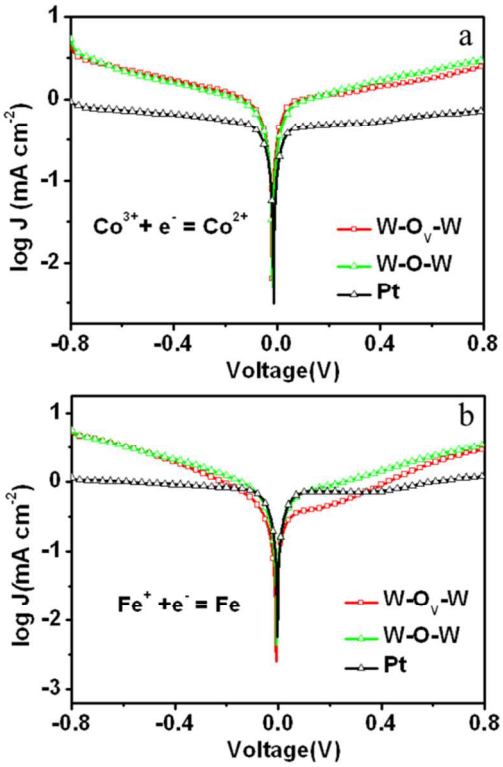

Figure 3. Tafel curves measured by the two identical electrodes based on three different catalytic electrodes for $Co(bpy)_3^{2+}/Co(bpy)_3^{3+}$ and Fc/Fc^+ redox mediators.

Table 1. Electrochemical parameters based on three different catalytic electrodes for $Co(bpy)_3^{2+}/Co(bpy)_3^{3+}$ and Fc/Fc^+ redox mediators, utilizing the two identical catalytic electrode

Redox mediators	CEs	E_O(mV)[a]	E_R (mV)[b]	ΔE_P(mV)	J_0	R_s(Ω)	R_{ct}(Ω)	Z_N(Ω)
$Co(bpy)_3^{2+}/Co(bpy)_3^{3+}$	W-O_V-W	584	426	158	0.55	16.31	2.33	8.27
	W-O-W	584	426	158	0.46	16.32	3.80	14.49
	Pt	582	429	153	0.32	9.26	3.20	15.81
Fc/Fc^+	W-O_V-W	675	454	221	0.39	14.86	2.49	16.58
	W-O-W	656	467	189	0.55	14.70	2.40	12.07
	Pt	614	491	123	0.70	11.92	1.99	11.25

a E_O stands for the position of oxidation peak at relative negative couple in CV.
b E_R stands for the position of reduction peak at relative negative couple in CV.

To further investigate the electrocatalytic properties of $Co(bpy)_3^{2+}/Co(bpy)_3^{3+}$ and Fc/Fc^+ redox mediators on SOVs of $W_{18}O_{49}$ in devices, DSCs were assembled using $Co(bpy)_3^{2+}/Co(bpy)_3^{3+}$ and Fc/Fc^+ redox mediators. Given the different mass transports and matches with dyes, different thicknesses of TiO_2 films and dyes were selected for the different redox mediators. Photocurrent density-voltage (J–V) curves were obtained for these DSCs based on W-O_V-W, W-O-W, and Pt under AM 1.5, 100 mW cm^{-2} simulated illumination, as shown in Figure 4. The detailed photovoltaic parameters are shown in Table 2. For $Co(bpy)_3^{2+}/Co(bpy)_3^{3+}$ redox mediator, the performance of DSCs based on W-O_V-W and W-O-W CEs can comparable to that based on Pt. After SOVs filling, PCEs was slightly decreased. This slightly decrement was mainly attributed to the reduction of the fill factor (FF) and current density. For Fc/Fc^+ redox mediator, the serious recombination between Fc^+

Cite this: DOI: 10.1039/c0xx00000x

www.rsc.org/xxxxxx

ARTICLE TYPE

and bare FTO of the photo anode caused the low voltage and *FF*, as shown in Figure S5a. The compact TiO_2 blocking layer

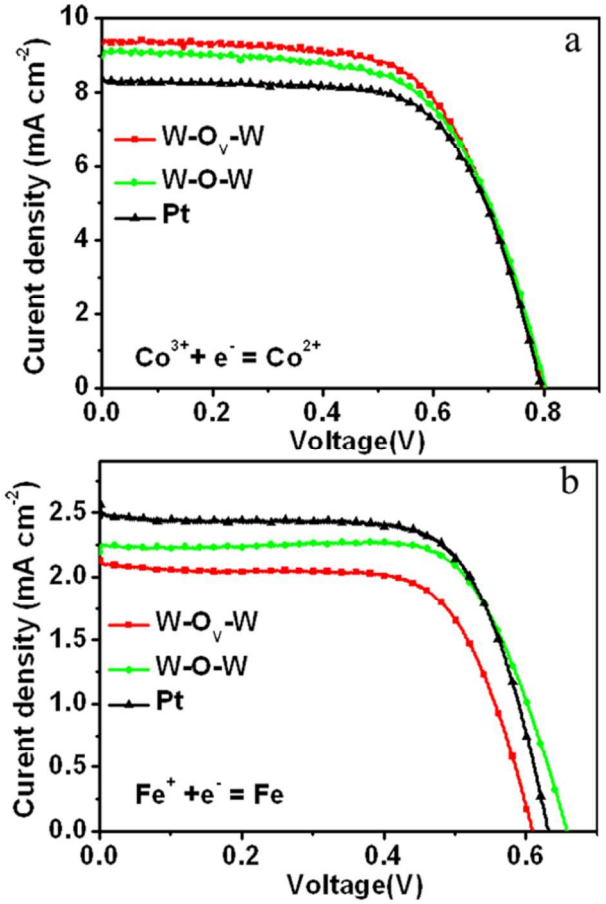

Figure 4. Photocurrent density - voltage curves of DSCs utilizing three different catalytic electrodes for $Co(bpy)_3^{2+}/Co(bpy)_3^{3+}$ and Fc/Fc^+ redox mediators. a) and b) are corresponded to *J-V* plots based on $Co(bpy)_3^{2+}/Co(bpy)_3^{3+}$ and Fc/Fc^+ redox mediators, respectivly.

efficiently inhibited the recombination between Fc^+ and bare FTO of the photo anode, as indicated by the dark current (Figure S5b). Although the PCEs based on Fc/Fc^+ were low, as shown in Figure 4b, we could see that the parameters of DSCs base on W-O_V-W and W-O-W were approaching to that of Pt. The PCEs slightly increased from 0.90% to 1.11 % after SOVs filling. This result was agreed with results of CV and Tafel.

Using the same symmetrical cells as in the case of Tafel polarization, EIS measurements[27] were performed to investigate the impedance between CEs and electrolytes based on redox mediators. Theoretically, each curve is composed of two irregular semicircles. The first one arises from the R_{ct} at the CE/electrolyte interface. The second semicircle results from the Nernst diffusion impedance (Z_N) of the redox mediators within the electrolyte. Moreover, the high frequency intercept on the real axis is the series resistance (R_s). The R_s values were obtained by fitting Nyquist plots with the "Z-view",[9] a well-known software, based on an equivalent circuit diagram (Figure 5a). The fitting results of

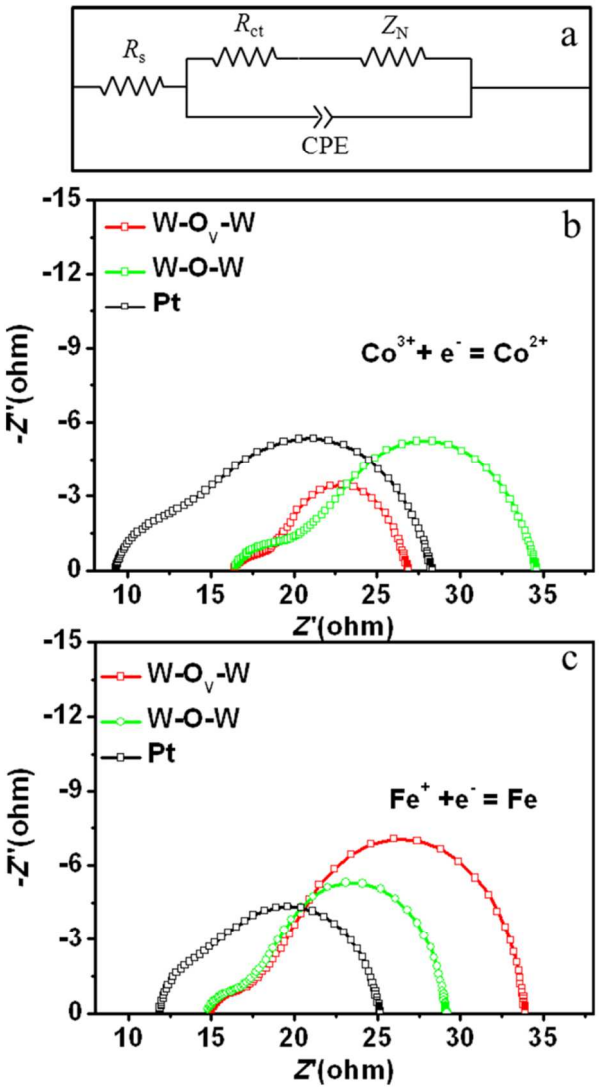

Figure 5. Nyquist plots measured by the two identical electrodes based on on three different catalytic electrodes for $Co(bpy)_3^{2+}/Co(bpy)_3^{3+}$ and Fc/Fc^+ redox mediators. a) equivalent circuit diagram for symmetrical cells fabricated with two identical counter electrodes; b) and c) are corresponded to nyquist plots of $Co(bpy)_3^{2+}$/ $Co(bpy)_3^{3+}$and Fc/Fc^+, respectivly.

the Nyquist plots are listed in Table 1. For $Co(bpy)_3^{2+}$/ $Co(bpy)_3^{3+}$, the R_s values for $W_{18}O_{49}$ catalysts before and after SOVs filling were almost the same but larger than that of the Pt CE. The R_{ct} values for W-O_V-W and W-O-W CEs were small and comparable to that of Pt, which confirmed that they had high electrocatalytic activity. For Fc/Fc^+, the R_{ct} values for W-O_V-W and W-O-W CEs was 2.49 Ω and 2.40Ω, respectively. The slight decrement of R_{ct} for Fc/Fc^+ after SOVs filling was observed.

Table 2. Photovoltaic parameters of DSCs based on three different catalytic electrodes for $Co(bpy)_3^{2+}/Co(bpy)_3^{3+}$ and Fc/Fc^+ redox mediators under AM 1.5, 100 mW cm^{-2} simulated illumination

Electrolyte/Dye	Catalysts	Film(μm)[a]	V_{oc}(V)	J_{sc}(mA/cm^2)	*FF*	PCE (%)
$Co(bpy)_3^{2+}/Co(bpy)_3^{3+}$//YD2-*o*-C8[b]	W-O_V-W	5+2	0.80	9.26	0.67	4.85
	W-O-W	5+2	0.81	8.89	0.65	4.69
	Pt	5+2	0.80	8.55	0.66	4.49
Fc/Fc^+//N719[c]	W-O_V-W	2+2	0.42	1.74	0.23	0.17
	W-O-W	2+2	0.34	1.71	0.25	0.15
	Pt	2+2	0.45	0.77	0.31	0.10
	W-O_V-W	B+2+2	0.61	2.16	0.68	0.90
	W-O-W	B+2+2	0.66	2.18	0.75	1.08
	Pt	B+2+2	0.63	2.50	0.69	1.11

[a] Film thickness is measured in x μm(transparent)+y μm(scattering); B stands for compact TiO_2 blocking layer
[b] YD2-*o*-C8 stands for [5,15-bis(2,6-dioctoxyphenyl)-10-(bis(4-hexylphenyl)amino)-20-(4-carboxyphenyl ethynyl)porphyrinato] Zinc(II)
[c] N719 stands for di-tetrabutylammonium-cis-bis(isothiocyanato)bis(2,2′-bipyridyl-4,4′-dicarboxylato) ruthenium(II)

The explanation for the different effects of SOVs on the electrocatalytic properties for $Co(bpy)_3^{2+}/Co(bpy)_3^{3+}$ and Fc/Fc^+ redox mediators is as follows. The diverse effects may have originated from the large and steric structure of $Co(bpy)_3^{2+}/Co(bpy)_3^{3+}$ and Fc/Fc^+ redox mediators and the adsorption site. As we all know, small molecules of iodine are preferentially adsorbed on metal atoms rather than on nonmetallic atoms in an inorganic complex.[28] Thus, the iodine molecules should be adsorbed on top of W atoms sourced from the abundant SOVs for the subsequent catalysis. Therefore, the electrocatalytic activity of I^-/I_3^- is notably affected by the abundant SOVs.[8, 19, 20] However, the SOVs are too small to anchor the large volumes of steric redox mediators ($Co(bpy)_3^{3+}$ and Fc), as shown in Schemes 1a. Thus, their electrocatalytic activity is slightly susceptible to SOVs. In addition, the strong metal properties of the center iron atom in the ferrocene redox mediator may facilitate its preferentially adsorbance on nonmetal atoms rather than on metallic atoms in an inorganic complex, as shown in Scheme 1b. The details for this mechanism are currently under investigation.

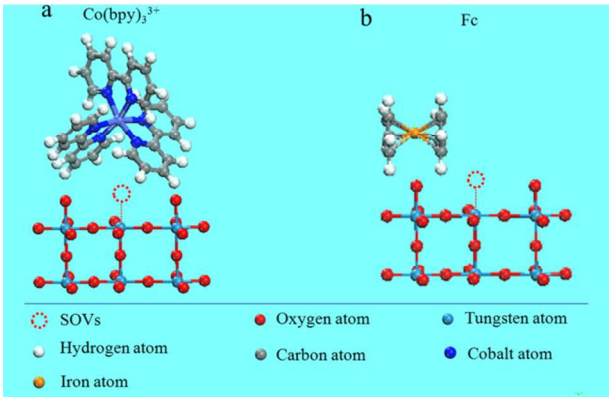

Scheme 1. Schematic diversity of adsorbption for $Co(bpy)_3^{3+}$ and Fc redox meditors on SOVs of $W_{18}O_{49}$.

Conclusions

In summary, we investigated the electrocatalytic properties of cobalt complex and ferrocenium redox mediators on SOVs of $W_{18}O_{49}$ in DSCs. We found that $W_{18}O_{49}$ NWs exhibited good electrocatalytic activity for $Co(bpy)_3^{2+}/Co(bpy)_3^{3+}$ and Fc/Fc^+ reduction reaction and were comparable to Pt. Results revealed different electrocatalytic properties of $Co(bpy)_3^{2+}/Co(bpy)_3^{3+}$ and Fc/Fc^+ on the SOVs located on the surface of $W_{18}O_{49}$ NWs. Unlike notable dependence on the SOVs for small I^-/I_3^-, the electrocatalytic activities for larger redox mediators with steric molecular configurations (cobalt complex, ferrocenium) were less dependence on the SOVs. The reduction reaction activities of the cobalt complex slightly decreased after SOVs filling. However, the reduction reaction activity of Fc/Fc^+ slightly increased after SOVs filling. These findings are helpful to understand the heterogeneous catalytic reactions on the surface of transition metal complex for different redox mediators and can accelerate rational search for highly active catalysts for different redox mediators.

Acknowledgements

This work was financially supported by National Natural Science Foundation of China (Grant no. 51273032 and 91333104), International Science & Technology Cooperation Program of China (Grant No. 2013DFA51000).

Notes and references

[a] *State Key laboratory of Fine Chemicals, School of Chemistry, Dalian*

Cite this: DOI: 10.1039/c0xx00000x

www.rsc.org/xxxxxx

ARTICLE TYPE

University of Technology, Dalian, China.
[b] Graduate School of Life Science and Systems Engineering, Kyushu Institute of Technology, 2-4 Hibikino, Wakamatsu, Kitakyushu, Fukuoka, 808-0196, Japan.
** Corresponding authors: tinglima@dlut.edu.cn; shiyantao@dlut.edu.cn*

1. M. Gratzel, *Nature*, 2001, **414**, 338-344.
2. K. Maeda, *Acs Catalysis*, 2013, **3**, 1486-1503.
3. T. Stergiopoulos and P. Falaras, *Advanced Energy Materials*, 2012, **2**, 616-627.
4. B. Oregan and M. Gratzel, *Nature*, 1991, **353**, 737-740.
5. A. Yella, H.-W. Lee, H. N. Tsao, C. Yi, A. K. Chandiran, M. K. Nazeeruddin, E. W.-G. Diau, C.-Y. Yeh, S. M. Zakeeruddin and M. Graetzel, *Science*, 2011, **334**, 629-634.
6. M. Wang, C. Graetzel, S. M. Zakeeruddin and M. Graetzel, *Energy & Environmental Science*, 2012, **5**, 9394-9405.
7. H. McDaniel, N. Fuke, N. S. Makarov, J. M. Pietryga and V. I. Klimov, *Nature Communications*, 2013, **4**.
8. H. Zhou, Y. Shi, L. Wang, H. Zhang, C. Zhao, A. Hagfeldt and T. Ma, *Chemical Communications*, 2013, **49**, 7626-7628.
9. M. Wang, A. M. Anghel, B. Marsan, N.-L. C. Ha, N. Pootrakulchote, S. M. Zakeeruddin and M. Graetzel, *Journal of the American Chemical Society*, 2009, **131**, 15976-+.
10. F. Gong, H. Wang, X. Xu, G. Zhou and Z.-S. Wang, *Journal of the American Chemical Society*, 2012, **134**.
11. Y. Hou, D. Wang, X. H. Yang, W. Q. Fang, B. Zhang, H. F. Wang, G. Z. Lu, P. Hu, H. J. Zhao and H. G. Yang, *Nature Communications*, 2013, **4**.
12. H. Zheng, J. Z. Ou, M. S. Strano, R. B. Kaner, A. Mitchell and K. Kalantar-zadeh, *Advanced Functional Materials*, 2011, **21**.
13. F. Verpoort, L. Fiermans, A. R. Bossuyt and L. Verdonck, *Journal of Molecular Catalysis*, 1994, **90**, 43-52.
14. B. F. Sels, D. E. De Vos and P. A. Jacobs, *Angewandte Chemie-International Edition*, 2005, **44**, 310-313.
15. J. Engweiler, J. Harf and A. Baiker, *Journal of Catalysis*, 1996, **159**, 259-269.
16. J. Macht, C. D. Baertsch, M. May-Lozano, S. L. Soled, Y. Wang and E. Iglesia, *Journal of Catalysis*, 2004, **227**, 479-491.
17. Y. Rezgui and M. Guemini, *Applied Catalysis a-General*, 2005, **282**, 45-53.
18. M. Wu, X. Lin, A. Hagfeldt and T. Ma, *Chemical Communications*, 2011, **47**, 4535-4537.
19. I. Jeong, C. Jo, A. Anthonysamy, J.-M. Kim, E. Kang, J. Hwang, E. Ramasamy, S.-W. Rhee, J. K. Kim, K.-S. Ha, K.-W. Jun and J. Lee, *Chemsuschem*, 2013, **6**, 299-307.
20. L. Cheng, Y. Hou, B. Zhang, S. Yang, J. W. Guo, L. Wu and H. G. Yang, *Chemical Communications*, 2013, **49**, 5945-5947.
21. C. Guo, S. Yin, M. Yan, M. Kobayashi, M. Kakihana and T. Sato, *Inorganic Chemistry*, 2012, **51**.
22. N. Papageorgiou, W. F. Maier and M. Gratzel, *Journal of the Electrochemical Society*, 1997, **144**, 876-884.
23. G. Q. Wang, R. F. Lin, Y. Lin, X. P. Li, X. W. Zhou and X. R. Xiao, *Electrochimica Acta*, 2005, **50**, 5546-5552.
24. S. M. Feldt, E. A. Gibson, E. Gabrielsson, L. Sun, G. Boschloo and A. Hagfeldt, *Journal of the American Chemical Society*, 2010, **132**, 16714-16724.
25. S. Ito, T. N. Murakami, P. Comte, P. Liska, C. Graetzel, M. K. Nazeeruddin and M. Graetzel, *Thin Solid Films*, 2008, **516**, 4613-4619.
26. H. Yu, S. Zhang, H. Zhao, B. Xue, P. Liu and G. Will, *Journal of Physical Chemistry C*, 2009, **113**, 16277-16282.
27. J. Bisquert, M. Graetzel, Q. Wang and F. Fabregat-Santiago, *Journal of Physical Chemistry B*, 2006, **110**, 11284-11290.
28. Y. Sining, Z. Hong, P. Huihai, C. Junhong, A. Hagfeldt and M. Tingli, *Advanced Energy Materials*, 2013, **3**, 1407-1412.